GABA_A α6-Containing Receptors Are Selectively Compromised in Cerebellar Granule Cells of the Ataxic Mouse, Stargazer*

Helen L. Payne[‡,1,2], **William M. Connelly**[§,1,3], **Jane H. Ives**[‡], **Reinhard Lehner**[¶,‖,4], **Birgit Furtmuller**[¶,‖], **Werner Sieghart**[¶,‖], **Priyanka Tiwari**[‡], **John M. Lucocq**[**,5], **George Lees**[§,3], and **Christopher L. Thompson**[†,‡]

[‡]Centre for Integrative Neurosciences, School of Biological and Biomedical Sciences, Science Research Laboratories, Durham University, South Road, Durham DH1 3LE, United Kingdom [¶]Centre for Brain Research, Medical University Vienna, Spitalgasse 4, Austria [‖]Section for Biochemical Psychiatry, University Clinic for Psychiatry, A-1090 Vienna, Austria [**]School of Life Sciences, University of Dundee, Dundee DD1 5EH, Scotland, United Kingdom [§]Department of Pharmacology and Toxicology, Otago School of Medical Sciences, University of Otago, P. O. Box 56, Dunedin, New Zealand

Abstract

Stargazer mice fail to express the $\gamma2$ isoform of transmembrane a-amino-3-hydroxyl-5-methyl-4-isoxazolepropionate (AMPA) receptor regulatory proteins that has been shown to be absolutely required for the trafficking and synaptic targeting of excitatory AMPA receptors in adult murine cerebellar granule cells. Here we show that $30 \pm 6\%$ fewer inhibitory γ-aminobutyric acid, type A (GABA_A), receptors were expressed in adult stargazer cerebellum compared with controls because of a specific loss of GABA_A receptor expression in the cerebellar granule cell layer. Radioligand binding assays allied to *in situ* immunogold-EM analysis and furosemide-sensitive tonic current estimates revealed that expression of the extrasynaptic ($a6\beta x\delta$) $a6$-containing GABA_A receptor were markedly and selectively reduced in stargazer. These observations were compatible with a marked reduction in expression of GABA_A receptor $a6$, δ (mature cerebellar granule cell-specific proteins), and $\beta3$ subunit expression in stargazer. The subunit composition of the residual $a6$-containing GABA_A receptors was unaffected by the stargazer mutation. However, we did find evidence of an ~4-fold up-regulation of $a1\beta\delta$ receptors that may compensate for the loss of $a6$-containing GABA_A receptors. PCR analysis identified a dramatic reduction in the steady-state level of $a6$ mRNA, compatible with $a6$ being the primary target of the stargazer mutation-mediated GABA_A receptor abnormalities. We propose that some aspects of assembly, trafficking, targeting, and/or expression of extrasynaptic $a6$-containing GABA_A receptors in cerebellar granule cells are selectively regulated by AMPA receptor-mediated signaling.

[2]To whom correspondence should be addressed: School of Biological and Biomedical Sciences, Durham University, Science Research Laboratories, South Road, Durham, DH1 3LE, UK. Tel.: 44-191-334-1312; Fax: 44-191-334-1201; H.L.Payne@durham.ac.uk..

[†]This paper is dedicated to the memory of Dr. Christopher L. Thompson, an accomplished neuroscientist, an inspirational colleague, and a valued friend, who died on June 5, 2007.
[1]Both authors contributed equally to this work.
[3]Supported by an Otago Research Grant and the New Zealand Neurological Foundation.
[4]Supported by the Austrian Science Fund Grant P17203.
[5]Supported by the Wellcome Trust, Research Leave Fellowship 059767/Z/99/Z, and Tenovus, Scotland, UK.
[7]P. Tiwari and C. L. Thompson, unpublished observations.
[8]H. L. Payne, J. H. Ives, and C. L. Thompson, manuscript in preparation.

The stargazer (*stg*) mutant mouse arose by virtue of a spontaneous viral transposon insertion into the *stargazin* gene (1). The mutation results in premature transcriptional arrest of the gene and complete ablation of its translation (2, 3). From postnatal day 14 onward *stg* mice display phenotypic consequences of the mutation that include head tossing (inner ear defect (1)), ataxia, impaired conditioned eyeblink reflex (cerebellar defects (4, 5)), and absence epilepsy (6). Stargazin is the $\gamma 2$ isoform of the family of transmembrane AMPA[6] receptor (AMPAR) regulatory proteins (TARPs) that are involved in AMPAR synaptic targeting and/ or surface trafficking (7, 8). TARP $\gamma 2$ is reported to be heavily expressed in the cerebellum (2, 9) where it is largely restricted to the cerebellar granule cells (CGCs), neurons that normally exclusively express the TARP $\gamma 2$ isoform of TARPs. Consequently, mossy fiber-CGC synapses in *stg* are bereft of AMPARs and are subsequently electrically silent (7) leading to a CGC-specific deficit in brain-derived neurotrophic factor (BDNF) expression and signaling (4). Considerable research interest has recently focused on the ability of inhibitory GABAergic networks to adapt to changes on the strength of their excitatory inputs (10-13) and any accompanying changes in BDNF/TrkB signaling (14-16). Interestingly, GABAR expression in CGCs has been shown previously to be impaired in *waggler* mice, which also arbor a mutated *stargazin* gene (17). The GABAR channel kinetics recorded in adult *waggler* CGCs were comparable with those expressed in CGCs of juvenile control mice (18) implying that the *waggler* mutation resulted in developmental arrest of CGCs that included restriction of GABAR maturation to that expected in juvenile neurons. This appeared to correlate with our previous data that showed that expression of the GABAR $\alpha 6$

---

[6]The abbreviations used are:

AMPA α-amino-3-hydroxyl-5-methyl-4-isoxazolepropionate

BZ-SR   benzodiazepine agonist-sensitive Ro15-4513 receptor

BZ-IS   benzodiazepine-insensitive

CGCs   cerebellar granule cells

GABAR γ-aminobutyric acid type A receptor

sIPSC   spontaneous inhibitory postsynaptic current

TARP   transmembrane AMPA receptor

GABA$_A$ aminobutyric acid, type A

AMPAR   AMPA receptor

RT   reverse transcriptase

BDNF   brain-derived neurotrophic factor

PBS   phosphate-buffered saline

NMDA   *N*-methyl-D-aspartic acid

aCSF   artificial cerebrospinal fluid

pS   picosiemen

pF   picofarad

subunit and the BZ-IS subtype of GABARs, markers of mature CGCs (19-22), were down-regulated in *stg* cerebellum (23). Here we have extended these earlier studies by using a more appropriate background strain of mice and including a more extensive analysis of receptor expression thus revealing information about the full complement of GABARs predicted to be expressed in the cerebellum and to evaluate whether the abnormalities in GABAR expression are restricted to distinct cellular and subcellular domains. Here we also provide evidence that the effects of the stargazer mutation on GABAR expression are largely restricted to CGCs. Furthermore, we have revealed that it is the $\alpha6$ subunit-containing GABAR subtypes that are selectively affected by the mutation, and these include not only the synaptic $\alpha6$ subunit-containing GABAR subtypes ($\alpha6\beta x\gamma2$ and $\alpha1\alpha6\beta x\gamma2$) but also the extrasynaptic, tonic inhibition-conferring $\alpha6\beta x\delta$ receptors (10, 24, 25), the latter being responsible for eliciting >97% of GABAR-mediated inhibition in CGCs and thus pivotal to information transfer in the cerebellum (26). The abundance and distribution of the GABAR $\gamma2$ subunit and the number of receptors that it contributes to are largely unaffected, as is the developmental maturation profile of the BZ-S subtype of cerebellar GABARs. Thus, our data imply that AMPA receptor activity has selective effects on GABAR subtypes expressed in cerebellar granule cells that may underpin homeostatic GABAergic responses to neuronal excitability.

EXPERIMENTAL PROCEDURES

Materials

Hyperfilm, horseradish peroxidase-linked secondary anti-rabbit antibodies, and [³H]flunitrazepam were purchased from Amersham Biosciences. Vectastain *Elite* ABC immunohistochemistry kits were purchased from Vector Laboratories (Peterborough, UK). Horseradish peroxidase-linked anti-goat secondary antibody was obtained from Pierce. Mammalian cell protease inhibitor mixture was purchased from Sigma. [³H]Muscimol and [³H]Ro15-4513 were purchased from PerkinElmer Life Sciences. Flunitrazepam, Ro15-1788, and Ro15-4513 were gifts from Hoffmann-La Roche. RNAzol B was purchased from Biogenesis (Poole, Dorset, UK). Moloney murine leukemia virus reverse transcriptase, recombinant RNasin ribonuclease inhibitor, dNTPs, and 100-bp DNA ladder were from Promega (Southampton, Hampshire, UK). Random primers and sequence-specific PCR primers were from Invitrogen. *Taq* polymerase and *Taq* polymerase buffer were from HT Biotechnology (Cambridge, Cambridgeshire, UK). All other materials were purchased from commercial sources.

Animals

Wild-type (C3B6Fe⁺; +/+), heterozygous (C3B6Fe⁺; +/*stg*), and homozygous stargazer mutant mice (C3B6Fe⁺; *stg*/*stg*) were obtained from heterozygous breeding pairs originally obtained from The Jackson Laboratory (Bar Harbor, ME) and maintained in the University of Durham vivarium on a 12-h light/dark cycle with food and water available *ad libitum*. Animal husbandry, breeding, and procedures performed during these experiments were conducted according to the Scientific Procedures Act 1986. We, in accordance with others (4, 27), have found no differences between wild-type and heterozygous mice in terms of their phenotype, behavior, or any of the molecular entities we have studied. We routinely use, therefore, a mixture of +/+ and +/*stg* mice brains in our control experiments. From this point forward we will refer to control derived tissue as +/+.

Radioligand Binding

Membranes prepared from control and *stg* cerebella were used for saturating binding assays using [³H]muscimol (1–77 nᴍ) and [³H]Ro15-4513 (0.3125–40 nᴍ) as described previously (23) and a single concentration of [³H]Ro15-4513 (20 nᴍ) for zolpidem-mediated

competitive displacement assays as described previously (11). Nonspecific [^{3}H]muscimol binding was determined in the presence of GABA (100 μ_M). Nonspecific [^{3}H]Ro15-4513 binding was determined in the presence of Ro15-1788 (10 μ_M). [^{3}H]Ro15-4513 binding in the presence of flunitrazepam (10 μ_M) allowed an estimation of the proportion of total specific [^{3}H]Ro15-4513-binding sites that were associated with either benzodiazepine full agonist-sensitive GABARs (BZ-SRs) or benzodiazepine full agonist-insensitive GABARs (BZ-ISRs). A minimum of eight radioligand concentrations was used for each saturation binding assay and performed at least in duplicate for each concentration of ligand used on 45–100 μg of protein/assay tube. Bound ligand was determined following rapid membrane filtration using a 24-sample Brandel Cell Harvester on polyethyleneimine (0.1% v/v)-treated GF/B filter paper. Statistical analysis of binding was performed using Graphpad Prism 3.0 software, and $p < 0.05$ was considered to be statistically significant.

Ligand Autoradiography

Procedures were essentially as described previously (28) with minor modifications. Mice were anesthetized with a lethal dose of pentobarbitone prior to transcardiac pressure perfusion, first with ice-cold phosphate-buffered saline (PBS)/NaNO$_2$ (0.1% w/v) for 3 min (10 ml/min) and then with ice-cold PBS/sucrose (10% w/v) for 10 min (10 ml/min). Brains were dissected and immediately frozen in isopentane (–40 °C) for 1 min. Brains were cryostat (Leica)-sectioned (–21 °C, 16 μm) in the horizontal plane and thawmounted onto polylysine-coated slides (BDH). Two control and two *stg* sections were thaw-mounted onto each slide thus enabling direct comparison of radiolabeling. Sections were airdried overnight, transferred to a desiccator, and stored at –20 °C until required.

Quantification of Receptor Autoradiographs

Autoradiographs and calibration standards were scanned at 1200 dpi using a flatbed scanner. Grayscale intensities were estimated using ImageJ software (National Institutes of Health, Bethesda). Calibration curves were constructed for each ligand/exposure period using ^{3}H standards, 0.1–109.4 nCi/mg (Amersham Biosciences) so grayscale intensity could be transformed into absolute radioactivity. Ten random subdomains of each cerebellar granule cell layer from a minimum of six comparable sections per mouse strain with a minimum of three mice per strain were used to yield an estimated mean intensity. Nonspecific binding values were subtracted from mean intensity values to resolve specific ligand binding. Statistical analysis was by Student's *t* test, and $p < 0.05$ was considered to be statistically significant.

Semi-quantitative RT-PCR Amplification

The steady-state level of GABAR α6 and δ subunits mRNAs and β-actin mRNA in control and *stg* cerebella were determined by semi-quantitative RT-PCR, essentially as described previously (11) with the following modifications.

Total RNA was extracted from cerebella using RNAzol B and resuspended in diethyl pyrocarbonate-treated water. The concentration and quality of the RNAs were determined by spectrophotometric analysis at 260 and 280 nm. Reverse transcription was performed in a total volume of 35 μl. Each reaction contained 1× Moloney murine leukemia virus reverse transcriptase reaction buffer (50 m$_M$ Tris-HCl, pH 8.3, 75 m$_M$ KCl, 3 m$_M$ MgCl$_2$,10 m$_M$ dithiothreitol); 1.14 m$_M$ each of dATP, dCTP, dGTP, dTTP; 40 units recombinant RNasin ribonuclease inhibitor and 3 μg of random hexamer. This was combined with total RNA of up to 1 μg and heated at 65 °C for 10 min. Reactions were rapidly chilled on ice before the addition of 400 units of Moloney murine leukemia virus reverse transcriptase and incubation at 42 °C for 90 min.

Oligonucleotide primers for amplification of mouse β-actin mRNA were 5′-ATTGAACATGGCATTGTTAC-3′ and 5′-CGAAGTCTAGAGCAACATAG-3′. Primers for the amplification of mouse GABAR α6 and δ subunits mRNAs were as described previously (11, 29). Amplicons of 271 bp (α6), 334 bp (δ), and 460 bp (β-actin) were predicted and detected.

PCRs were performed in a total volume of 25 μl. Each reaction contained (final concentration) 10 m$_M$ Tris-HCl, pH 9.0, 1.5 m$_M$ MgCl$_2$, 50 m$_M$ KCl, 0.1% Triton X-100, 0.4 m$_M$ dNTPs, 1 unit of *Taq* polymerase, and forward and reverse PCR primers. Five pmol of each primer was required for amplification of GABAR α6, and 25 pmol of each primer was required for amplification of β-actin and δ. Complementary DNA (2 μl), reversetranscribed from 1.0, 0.6, 0.4, or 0.2 μg of RNA, was amplified. Optimal PCR conditions were identified for each primer pair such that a single band of the expected size was produced, and the amount of product amplified was linear for at least three consecutive cDNA concentrations. The amplification protocol was as follows: 94 °C, 5 min followed by cycles of 94 °C for 45 s then 60 °C for 45 s (except 55 °C, 60 s for β-actin; 57 °C, 45 s for GABAR α6); 72 °C for 60 s (except 72 °C, 90 s for β-actin). The numbers of cycles were 24 for β-actin and 26 for GABAR α6 and δ subunits. Amplification products were resolved on 1.2% (w/v) agarose gels and stained with ethidium bromide. Amplified products were sized according to their migration with respect to the bands on a 100-bp DNA ladder. Gels were then analyzed using the Quantity One (4.0.3) software for the GelDoc 2000 system (Bio-Rad). Control experiments included running the amplification procedure with each primer pair in the absence of cDNA, or running samples that had not been reverse-transcribed. Neither gave a final product. For each set of cDNAs, a β-actin value was determined. This value was used accordingly to regulate the values determined for the GABAR subunit amplifications to account for inaccuracy in the spectrophotometric measurements of RNA used in cDNA synthesis.

Antibodies

The generation and purification of anti-peptide GABAR subunit-specific antibodies directed against α1 (amino acid residues Cys[1–14]) (11), α6-(Cys[1–15] (11)), β2-(351–405) (30), β3-(345–408) (31), γ2-(319–366) (32), and δ-(1–44) (28) have been described previously. Affinity-purified GABAR β2-(351–405), β3-(345–408), γ2-(319–366), and δ-(144) subunit-specific antibodies were supplied by Prof. Werner Sieghart, Medical University Vienna. Affinity-purified GABAR α1-(Cys[1–14]) subunit-specific antibodies used in immunohistochemical studies were provided by Professor F. A. Stephenson (School of Pharmacy, London, UK). Anti-NMDA receptor NR1 and NR2C/D subunit-specific antibodies were as described previously by us (33). Anti-β-actin antibody was purchased from Sigma.

SDS-PAGE and Western Blot Analysis

Control and *stg* mouse cerebella were homogenized individually using an Ultra-Turrax®, twice in a volume of 10 ml of homogenization buffer (10 m$_M$ Hepes, 1 m$_M$ EDTA, 300 m$_M$ sucrose) and once in 10 ml of washing buffer (10 m$_M$ Hepes, 1 m$_M$ EDTA), both containing one complete protease inhibitor mixture tablet per 50 ml of buffer (Roche Diagnostics), per cerebellum. Resulting pellets were finally resuspended in 6 ml of washing buffer.

SDS-PAGE was performed using the NuPAGE Western blotting system (Invitrogen), using 10% polyacrylamide gels in a discontinuous system. For estimation of the size of the proteins "MagicMarkTM XP Western Standards" (Invitrogen) were used in separate lanes. Equal amounts (containing 10 μg of protein) of the suspension were subjected to SDS-PAGE in different slots of the same gel. Proteins were blotted to polyvinylidene difluoride

membranes and detected by antibodies to the following subunits: GABAR α1-(328–382); α6-(317–371), β2-(351–405), β3-(345–408), γ2-(319–366), or δ-(1–44) (30, 34). Secondary antibodies (F(ab')2 fragments of goat anti-rabbit IgG, coupled to alkaline phosphatase (Axell, Westbury, NY), were visualized by the reaction of alkaline phosphatase with CDP-Star (Applied Biosystems, Bedford, MA). The chemiluminescent signal was quantified by densitometry after exposing the immunoblots to the Fluor-S multi-imager (Bio-Rad) and evaluated using the Quantity One quantitation software (Bio-Rad) and GraphPad Prism (Graph Pad Software Inc., San Diego). Quantification was performed by an independent investigator blind to the identity of the samples. The linear range of the detection system was established by measuring the antibody generated signal to a range of antigen concentrations. Under the experimental conditions used, the immunoreactivities were within the linear range, and this permitted a direct comparison of the amount of antigen per gel lane between samples (11, 35, 36). The amounts of individual GABAR subunits present in membranes from control and stargazer mice were compared in the same gel. Data were generated from several different gels per subunit and per mouse and expressed as means ± S.E. Student's unpaired t test was used for comparing groups, and significance was set at $p <$ 0.05.

To test for equal protein loading, in some experiments a monoclonal anti-β-actin antibody was included in the antibody solution, and the amounts of endogenous β-actin were quantitatively determined in a way analogous to GABAR subunits. Protein loading was comparable in different slots, and referring the data to the amounts of endogenous β-actin neither changed the results nor reduced variability.

Immunoprecipitation of GABARs

GABARs were solubilized from control and *stg* mouse cerebella using 6 ml of a deoxycholate buffer (0.5% deoxycholate, 0.05%, phosphatidylcholine, 10 m$_M$ Tris-HCl, pH 8.5, 150 m$_M$ NaCl, 1 Complete Protease Inhibitor Mixture tablet (Roche Diagnostics) per 50 ml per cerebellum. The suspension was homogenized using an Ultra-Turrax® and subsequently by pressing the suspension through a set of needles with increasingly smaller diameters using a syringe, followed by incubation under intensive stirring for 60 min at 4 °C. After centrifugation at $150,000 \times g$ for 45 min part of the clear supernatant (200–400 μg of protein) was used for subsequent immunoprecipitations either with 5 μg of anti-GABAR δ(1–44) or 20 μg of anti-GABAR α6-(317–371) antibodies overnight at 4 °C. Immunoprecipitin (20 μl) in IP-low buffer (50 μl) (containing 50 m$_M$ Tris-Cl, pH 8.0, 150 m$_M$ NaCl, 1 m$_M$ EDTA, and Triton X-100 (0.2% v/v), supplemented with 5% (w/v) dry-milk powder) was subsequently added and incubated for 2 h at 4°C. Precipitate was pelleted by centrifugation at $2700 \times g$ for 5 min, and the pellet was washed three times with 500 μl of IP-low buffer before being resuspended in 100 μl of SDS-PAGE sample buffer (NuPAGE Western blotting system; Invitrogen). Samples from control and *stg* were simultaneously subjected to SDS-PAGE, applying multiple samples of the same amount of protein from the same brain to one gel. Each Western blot was cut in strips, and two strips each from a gel containing control or *stg* material were probed simultaneously either with digoxigenized anti-α1-(1–9), anti-α6-(1–15), anti-γ2-(319–366), or anti-δ-(1–24) antibodies to reduce experimental variability. Primary antibodies were detected with anti-digoxigenin-alkaline phosphatase Fab fragments (Roche Diagnostics) and CDP-Star (Tropix, Bedford, MA). Immunoreactive proteins were visualized by chemiluminescence using the Fluor-S multi-imager (Bio-Rad) and were quantified using Quantity One (Bio-Rad) and GraphPad Prism (Graph Pad Software Inc., San Diego). The relative signal intensity of proteins stained with the different antibodies was compared within each gel and was referred to that of the precipitated subunit. The intensity ratios were then compared between receptors precipitated from control (+/+) and *stg* extracts.

Immunohistochemistry

Adult (2–6 months) control and *stg* mice were anesthetized with a lethal dose of pentobarbitone. The mice were transcardially perfused through the ascending aorta with ice-cold PBS, pH 7.4 containing $NaNO_2$ (0.1% w/v) for 3 min at 10 ml/min. The perfusate was then exchanged for ice-cold 4% (w/v) paraformaldehyde in phosphate buffer (0.1 M, pH 7.4), perfused for a further 20 min at 10 ml/min. Brains were dissected out and post-fixed in 4% (w/v) paraformaldehyde in phosphate buffer (0.1 M, pH 7.4, 4 °C) for 24 h. The brains were then transferred to PBS containing 10% (w/v) sucrose for 48 h, 4 °C, exchanging the PBS/sucrose every 12 h. Brains were frozen in isopentane (−70 °C) for 2 min and then cryostat-sectioned (30 μm) in the horizontal and sagittal planes. Sections were transferred to the wells of 24-well plates containing PBS/NaN_3 (0.02% w/v). Free-floating sections were immunohistochemically stained by standard methods (33). Briefly, unreacted paraformaldehyde was quenched by incubation, 30 min, in PBS/glycine (0.2% w/v, pH 7.4). Nonspecific binding sites were blocked with 10% goat serum in PBS/Triton X-100 (0.2% v/v). Sections were then exposed to GABAR subunit-specific primary antibodies at optimized concentrations (0.5 μg/ml (a1, β2, β3, γ2), 0.06 μg/ml (a6); 0.25 μg/ml (δ)) overnight at 4 °C. Sections were then stained using the Vectastain ABC *Elite* kit with 3,3-diaminobenzidine (0.5 mg/ml), 0.02% (v/v) H_2O_2 in Tris-buffered saline, pH 7.2, as horseradish peroxidase substrate.

Quantitative Immunoelectron Microscopy

Brains were perfusion-fixed as described for immunohistochemistry with the following modifications. Brains were perfusion-fixed with either 8% paraformaldehyde in 0.2 M Hepes, pH 7.2 (Hepes buffer), or 4% paraformaldehyde, 0.1% glutaraldehyde in Hepes buffer or 0.5% glutaraldehyde in Hepes buffer. The data presented here were derived from 0.5% glutaraldehyde in Hepes buffer-fixed sections as these conditions offered the best compromise between immunogold signal and preservation of morphology. Brains were dissected out and stored in fixative. Cerebellar cortex from the vermis region was cut into 0.5-mm sized blocks. These were cryoprotected in 2.3 M sucrose, 20% (v/v) polyvinylpyrrolidone (40 kDa) in PBS, mounted on iron panel pins, and frozen in liquid nitrogen. Frozen tissue was sectioned with a diamond knife on a Leica ultracryomicrotome and mounted on pioloform/carbon-coated EM support grids. Immunogold labeling was as follows: grid-mounted sections were incubated for 5 min on drops of 0.5% (w/v) fish skin gelatin in PBS (PBS/gelatin; Sigma) and then for 5 min on 0.1 M ammonium chloride in PBS. Sections were then incubated in anti-GABAR a6-(Cys[1–15]) subunit-specific antibodies (2.13 μg/ml) in PBS/gelatin for 30 min, washed in PBS, and then incubated on protein A-Gold (8 nm particle size; prepared as described previously (37)). After final washes in PBS and distilled water, the sections were embedded and contrasted in methyl cellulose/uranyl acetate. Labeling was quantified using stereologic techniques to estimate the membrane profile length of each membrane compartment, including granular cell plasma membrane, dendrite membrane, and Golgi-granule cell synapses as described previously (38). Pictures were recorded at systematically placed locations with a random start at ×10,000 magnification on photographic film. Images were scanned at 1000 dpi, displayed in Adobe Photoshop 5.5, and overlaid with an electronically generated square lattice grid with spacing of 0.5 μm. Area of compartments was estimated from $\pi/4 \times I \times d$, in which I is the sum of intersections with relevant membrane profiles, and d is the grid spacing. Typical counts of intersection hits and gold in a control experiment were, respectively, 444 and 72 for granule cell plasma membrane, 165 and 44 for dendrite membrane, and 148 and 11 for Golgi-granule cell synapses.

Protein Determinations

Protein concentrations were determined according to the method of Lowry *et al.* (39) employing bovine serum albumin as standard for calibration.

Electrophysiology

33–57-Day-old male mice were anesthetized with pentobarbital (120 mg/kg, intraperitoneal) and decapitated. Brains were rapidly dissected out into ice-cold modified artificial CSF (aCSF) of the following composition (in m_M): 248 sucrose, 3 KCl, 2 $MgCl_2$, 1 $CaCl_2$, 1.25 NaH_2PO_4, 26 $NaHCO_3$, and 10 glucose (saturated with 95% O_2, 5% CO_2). Sagittal slices of the cerebellum, 200 μm thick, were cut using a vibratome (VT1000S; Leica, Ora, Italy) and placed in a holding chamber at 35 °C in aCSF of the following composition (in m_M): 124 NaCl, 3 KCl, 1 $MgCl_2$, 2 $CaCl_2$, 1.25 NaH_2PO_4, 26 $NaHCO_3$, 10 glucose, 1 sodium ascorbate, 3 sodium pyruvate (bubbled with 95% O_2, 5% CO_2) for 30 min and then allowed to return to room temperature. Slices were incubated under these conditions for a further 30 min before recording began. Slices were placed in a custom-made recording chamber on the stage of a differential interference contrast microscope (E600FM DIC; Nikon, Tokyo, Japan) and perfused with room temperature (20–24 °C) aCSF containing 20 μ_M Na-CNQX and 10 μ_M D-AP5 at ~2 ml/min. Visually identified granule cells were patched with thick wall borosilicate electrodes (3-5 megohms) filled with the following solution (in m_M): 120 CsCl, 10 Hepes, 10 EGTA, 5 QX-314 (2(triethylamino)-*N*-(2,6-dimethylphenyl) acetamine), 4 sodium phosphocreatine, 1 Na_2ATP, 0.3 LiGTP, pH 7.35, with CsOH (held at −70 mV). Input conductance was measured using a 200-ms, 15–25-mV hyperpolarizing step. Cells were held for at least 5 min to allow the pipette solution to dialyze the cell and the series resistance to equilibrate over which time an inward current slowly developed (presumably as a result of increase $[Cl^-]_i$). The control phase of recording did not begin until the inward current reached equilibrium. If the series resistance increased above 30 megohms or changed by 10% during the course of a recording, the data from that cell were excluded from additional analysis. Series resistance was compensated to 80%. Data were filtered at 3 kHz and logged at 10 kHz (micro 1401; Cambridge Electronics Design, Cambridge, UK) to Spike 4 software. We used two-tailed, Mann-Whitney and Wilcoxon matched pairs test, and $p < 0.05$ was regarded as significant. Data are shown as median (25th percentile, 75th percentile). Furosemide and zolpidem were dissolved in Me_2SO. Me_2SO concentrations were 0.01% (v/v) in both control and drug aCSF.

RESULTS

Comparative Pharmacological Profile of Cerebellar GABARs Expressed in Control and stg Mice

[³H]Muscimol Binding to Cerebellar Membrane Homogenates—The total number of GABARs expressed in the cerebella of adult control and *stg* mice was determined by [³H]muscimol binding to well washed, frozen-thawed cerebellar membrane homogenates. Muscimol binds to the principal and mutually exclusive γ2- *and* δ-containing subtypes of GABARs that constitute 98% of all GABARs expressed in the adult mouse cerebellum (34). Saturation binding studies revealed that the total number of specific [³H]muscimol binding sites (B_{max}) was significantly lower, by $30 \pm 6\%$, in *stg* compared with control indicating a change in the GABAR population (Fig. 1). The K_D for muscimol binding was not significantly different between control and *stg* being 3.0 ± 0.9 and 3.6 ± 0.7 n_M, respectively (Fig. 1), indicating no overall difference in receptor affinity for muscimol between the mouse strains.

[³H]Muscimol Binding to Unfixed Cerebellar Membrane Sections (in Situ Autoradiography)—By *in situ* autoradiography, [³H]muscimol selectively highlights α6-

containing GABARs in the cerebellum ($a6\beta\gamma2$, $a1a6\beta\gamma2$, $a6\beta\delta$ and $a1a6\beta\delta$ (28, 34, 40)). Unfixed brain sections were probed with a saturating dose (20 n_M) of [³H]muscimol (Fig. 2). A dramatic reduction in specific muscimol binding in the CGC layer of *stg* relative to controls was observed (reduced by $46 \pm 3\%$). The reduction in binding was uniform throughout all cerebellar lobules (Fig. 2).

[³H]Ro15-4513-Binding Sites ($\gamma2$-Containing GABARs)—We had previously reported that expression of total specific [³H]Ro15-4513-binding sites in the cerebellum of *stg* was not significantly different from that found in control mice (23). However, these initial studies were conducted with C57Bl/J6 mice as background controls, whereas the *stg* mouse was bred onto a C3B6 line. Recent data have identified mouse strain-dependent differences in CGC properties. We repeated these earlier studies but using phenotypically normal, age-matched +/+ and +/*stg* littermates of *stg/stg* mutants as controls (C3B6Fe +/+ and +/*stg*). Furthermore, we extended these earlier studies to include an evaluation of the abundance and distribution of [³H]Ro15-4513-binding sites in *stg* mice using *in situ* autoradiography. The current results are largely compatible with those of our previous study (23).

[³H]Ro15-4513 Binding to Cerebellar Membrane Homogenates—The total number of cerebellar [³H]Ro15-4513-binding sites (total number of $\gamma2$-containing GABARs) was only modestly affected by the mutation being reduced by $19 \pm 9\%$, equivalent to a reduction of ~$13 \pm 6\%$ of total GABARs (34), relative to control (Fig. 3). This reduction in [³H]Ro15-4513-binding sites was entirely accommodated by a selective reduction in expression of the BZ-IS subtype of $\gamma2$-containing GABARs, being reduced by $43 \pm 12\%$ (Fig. 3). The abundance of the BZ-S subtype of [³H]Ro15-4513-binding sites was not significantly affected by the stargazer mutation, B_{max} being 0.71 ± 0.08 (control) and 0.65 ± 0.06 (*stg*) pmol/mg protein (Fig. 3).

[³H]Ro15-4513 Binding to Unfixed Cerebellar Membrane Sections (in Situ Autoradiography)—When analyzed by *in situ* autoradiography, these deficits appeared restricted to the CGC layer. A comparable small reduction in total [³H]Ro15-4513-binding sites (by $10 \pm 4\%$) was detected (Fig. 4*A*) as was a comparable significant reduction in BZ-IS [³H]Ro15-4513-binding sites (by $21 \pm 7\%$) (Fig. 4*B*). These reductions were consistent across all cerebellar lobules and within individual lobules. Using [³H]flunitrazepam to highlight BZ-S receptors *in situ*, it was evident that BZ-S receptors were slightly more abundant in *stg* cerebellum than in controls (being $113 \pm 6\%$ of controls, Fig. 4*C*) ($p > 0.05$).

Is the Aberrant GABAR Expression Profile in stg Cerebellum Because of Arrested Development of This Brain Region?

Although the abundance of the BZ-S subtype of GABARs was not significantly affected by the stargazer mutation, we did not know whether the subunit composition of this subtype was different in *stg* compared with controls. It has been reported previously that the mutation of the *stargazin* gene in *waggler* mice resulted in arrested maturation of CGCs. The functional characteristics of GABARs expressed by CGCs of adult *waggler* mice were similar to those expressed in juvenile normal mice (7). One characteristic of the development of the cerebellum is the switch of the BZ-S subtype of GABARs from pharmacologically definable type II benzodiazepine-binding site (low affinity for the hypnotic agent zolpidem) to a type I benzodiazepine-binding site (high affinity for zolpidem). This is achieved by a developmental switch in the GABAR subunit expression profile preferring assembly of $a2/a3\beta x\gamma2$ receptors (type II BZ-SRs) in the juvenile cerebellum that transforms to assembly of receptors comprising largely $a1\beta x\gamma2$ subunits (type I BZ-SRs) in the adult cerebellum. Thus, we investigated whether BZ-S GABARs

were immature in *stg* cerebellum. Zolpidem competitively displaced >98% of [^{3}H]Ro15-4513 binding to BZ-S receptors expressed in both control and *stg* cerebellar membrane homogenates with IC_{50} values of 45 and 50 n$_M$ for control and *stg*, respectively, both compatible with high affinity type I BZ-SRs (Fig. 5). The displacement curve was predicative of binding to a single site. The IC_{50} for zolpidem displacement of [^{3}H]Ro15-4513 binding to BZ-S receptors expressed in cerebellar membranes from juvenile (postnatal day 9) control mice was ~282 n$_M$, which is compatible with the predominant expression of type II receptors in the cerebellum at this age (data not shown). Thus, our observations relating to GABAR expression cannot be attributed to a global effect of the mutation on cerebellar maturation. Furthermore, we tested whether the reported developmental switch in NMDA receptor subunit expression from NR2B, a characteristic of juvenile CGCs to NR2C, a marker of mature CGCs occurred. We found NR2B to be undetectable in adult *stg* cerebellar tissue but did detect NR2C,,7 confirming a developmental switch in the maturity of *stg* CGCs.

Immunohistochemical Mapping of Cerebellar GABAR Subunits in Control and stg Mice

We next investigated whether the changes in GABAR subtype expression were paralleled by changes in the distribution (immunohistochemistry, cerebellar sections) and/or abundance (quantitative immunoblotting, cerebellar membranes) of the principal GABAR subunits (a1, a6, β2, β3, γ2, δ) expected to be expressed in the mature cerebellum (41) of adult +/+ and *stg* mice. No overt changes in the cellular distribution were observed, although the intensity of staining (abundance) for GABAR a6, β2, β3, and δ subunits was clearly reduced in the CGC layer in *stg* mice relative to +/+ (Fig. 6). No consistent changes in the intensity of staining with GABAR a1 or γ2-specific antibodies were observed (Fig. 6). GABAR a6 and δ immunostaining was detected in all lobules of the *stg* cerebellum but was less intense compared with controls in both cases (Fig. 6) in accordance with the reduced expression of high affinity muscimol-binding sites by *in situ* autoradiography (Fig. 2) and BZ-IS receptors (Fig. 3 and Fig. 4*B*). Interestingly, the pattern of immunostaining of GABAR a6 in *stg* granule cells was different from that seen in the control mouse. The less intense punctate staining observed in *stg* cerebellar granule cells (Fig. 6) was similar to that found for synapse-targeted proteins such as the NMDA receptor NR2C subunit (33). Implying that the distribution of staining in control mouse cerebellum might reflect synaptic *and* extrasynaptic a6-containing receptors, whereas in *stg* only synaptic appeared to be highlighted, suggesting severely compromised expression of extrasynaptic a6-containing receptors, which include the a6βxδ subtype.

Changes in GABAR Composition in stg Cerebellum

Quantitative immunoblotting (Fig. 7 and Table 1) of cerebellar membranes from adult +/+ and *stg* using subunit-specific antibodies identified two pools of subunits, those whose expression level was dramatically affected by the mutation, *e.g.* a6 (49 ± 2% relative to control) and δ (52 ± 3% relative to control), whereas others, *e.g.* a1, were either modestly (85 ± 1% relative to control) or not significantly affected, *e.g.* γ2 (95 ± 4% relative to control). Furthermore, expression of NMDA receptor NR1 (129 ± 28%) and NR2D (101 ± 10%) subunits were refractory to the stargazer mutation. The quantitative estimations of the difference in GABAR subunit abundance in whole *stg* cerebella was paralleled by our qualitative estimations of their abundance in the CGC layer by immunohistochemistry where a6 and δ were clearly less prevalent in *stg* CGCs compared with controls, whereas a1 and γ2 appeared unaffected by the *stg* mutation (Fig. 6).

The dramatic loss of a6 and δ subunits in the cerebellum of *stg* as indicated by Western blot analysis could have been caused by a linear reduction of all a6- and δ-containing receptors without a change in the subunit composition of the remaining receptors. Alternatively, the

subunit composition of the remaining receptors additionally could have become changed. To investigate these alternatives, δ or α6 subunit-specific GABAR subpopulations were selectively immunoprecipitated from the cerebellum of +/+ and *stg* mice using the appropriate subunit-specific antibodies. Changes in co-association of α6, α1, and γ2 with δ subunits or of α1, γ2, and δ with α6 subunits were then quantified by comparing the protein staining of the respective subunits in δ- or α6-containing receptors of +/+ and *stg* cerebellum.

δ-Purified Cerebellar GABARs—As indicated in Table 2, when we screened δ-purified cerebellar GABARs, γ2 subunit was not detected, in accordance with previous results (30, 34). The degree of association of α6 subunits with δ receptors was similar in +/+ (45 ± 16%) and *stg* (40 ± 13%) cerebellum, whereas that of α1 subunits was dramatically *increased* in *stg* cerebellum (117 ± 11%), suggesting a change in the subunit composition of δ receptors.

α6-Purified Cerebellar GABARs—The degree of association of α1 (175 ± 12%), γ2 (138 ± 16%), and δ (133 ± 13%) subunits with α6 subunits was not significantly changed in *stg* cerebellum, suggesting no change in the composition of the remaining α6 receptors.

Steady-state Levels of α6 but Not δ mRNA Are Affected by the Stargazer Mutation—Our data thus far indicated that the stargazer mutation selectively compromised α6- and δ-containing GABAR expression. This suggested that the α6 subunit is the primary cause of the receptor reduction in *stg*, because ~50% of the α6 subunits are associated with γ2 and ~50% with δ subunits and because both of these receptor types seem to be equally affected. If δ were the primary cause, we would have not expect a reduction in receptors composed of α6 and γ2 (BZ-IS subtype, Fig. 3 and 4*B*). We therefore used semi-quantitative RT-PCR to investigate whether the mRNAs for GABAR α6 and δ were affected by the mutation. Fig. 7*B* shows that the steadystate level of α6 mRNA found in *stg* CGCs was significantly reduced (lower by 60 ± 6%) relative to +/+ (Fig. 7*B*). The steady-state level of δ mRNA was not significantly different between +/+ and *stg* (Fig. 7*B*).

Are Synaptic α6-Containing GABARs (e.g. α6βxγ2) and/or Extrasynaptic α6-Containing GABARs (e.g. α6βxδ) Compromised in stg?

Based on our radioligand binding data, there are 30% fewer GABARs expressed in the *stg* cerebellum than in controls. Because 98% of GABARs expressed in the mouse cerebellum can be subdivided into two mutually exclusive subpopulations comprising those that are γ2-containing (~70% of total GABARs (34)) and those that are δ-containing (~28% of total GABARs (34)) and that we detected only ~13 ± 6% reduction of the γ2-containing subpopulation ([^{3}H]Ro15-4513 binding, Fig. 3) of total GABARs, which was entirely attributable to down-regulation of the BZ-IS subtype (α6βxγ2-containing), implied that a sizeable pool of the α6βxδ-containing receptors was not expressed in *stg*. This extrapolation was supported by our *in situ* muscimol binding study (Fig. 2) and results of immunohistochemistry (Fig. 6) and immunoblotting (Table 1) using δ-specific antibodies. Because α6βxδ receptors are expressed exclusively at extrasynaptic sites of CGCs, we used our α6-specific antibody, which proved to be an effective probe for postembedding immunogold-cytochemistry on electron microscopic sections, to evaluate whether α6-containing receptors were compromised at CGC extrasynaptic and/or Golgi-CGC synaptic sites (Fig. 8). Clearly, extrasynaptic plasma membrane-targeted α6 subunit expression on granule cell bodies and dendrites was significantly down-regulated, being only 15 ± 3 and 5 ± 5% of control levels, respectively. Likewise, expression in Golgi-granule cell synapses was also significantly reduced to 32 ± 24% of control levels (Fig. 8).

The Tonic GABAR-mediated Conductance Is Mediated by Smaller Fraction of α6 Containing GABARs in stg Mice

Given that $\alpha6\beta x\delta$ GABARs likely mediated the tonic GABAR-mediated current in CGCs (10), we expected the loss of α6-containing GABARs in *stg* mice would result in a decrease in resting whole-cell conductance. Using whole-cell patch clamping in cerebellar brain slices, there was no difference in the membrane conductance of CGCs in *stg* and +/+ mice (+/+ 446 (interquartile range, 329, 560) pS/pF; *stg* 406 (330, 540) pS/pF; $n = 29$–33, $p = 0.7$, Mann Whitney test, data not shown). However, saturating concentrations of the α4/6 containing GABAR-selective antagonist furosemide (100 μ_M) (42, 43) produced a significantly smaller decrease in whole-cell conductance in *stg* mice (4% (−0.7, 8)) than their nonepileptic littermates (10% (8, 16); $n = 9$–11, $p = 0.011$, Mann Whitney test, Fig. 9, *a* and *b*), indicating that a smaller proportion of the tonic GABAR-mediated current is conducted by α6-containing GABARs. Zolpidem (3 μ_M) increased the decay time of spontaneous inhibitory postsynaptic currents recorded in CGC (data not shown) but did not produce a significant change in whole-cell conductance in either *stg* (0.7% (−3, 6), $n = 6$, $p = 0.6$, Wilcoxon matched pairs test) or +/+ mice (0.4% (−2, 2), $n = 6$, $p = 0.8$, Wilcoxon matched pairs test Fig. 9*c*) indicating that the tonic GABAR-mediated current is not mediated by $\alpha1/2/3\beta x\gamma2$-containing GABARs. The fact that there was no difference in resting whole-cell conductance makes it likely that *stg* mice develop a compensatory conductance to account for their lost tonic α6-containing GABAR-mediated current, in a similar fashion as has been shown in the CGCs of δ subunit knock-out mice (44).

DISCUSSION

The *stg* mutation selectively and completely ablates expression of TARPγ2 (3), a member of the TARP family of AMPAR synaptic targeting and/or trafficking proteins (7-9). Consequently, mossy fiber-cerebellar granule cell (CGC) synapses are silent to mossy fiber glutamate release because AMPARs are no longer trafficked to the CGC surface nor targeted to this synapse. The CGCs are therefore functionally deafferentiated and have consequently been shown to fail to express BDNF, which is an activity-dependent process (4, 27).

GABAR Plasticity

Inhibitory GABAergic networks have been shown to adapt to changes in the strength of their excitatory inputs (10-13) and any accompanying changes in BDNF/TrkB signaling (14-16). In electrically silent, BDNF-deficient CGCs of *stg*, we previously reported that GABAR receptor α6 and β3 subunits and BZ-IS ($\alpha6\beta x\gamma2$) receptors were down-regulated, whereas BZ-S receptors were unaffected (23). However, these previous studies failed to address whether the stargazer mutation affected the extrasynaptic $\alpha6\beta x\delta$ GABARs that are exclusively expressed by CGCs and that provide tonic inhibitory current to these neurons. These receptors are extremely important as they have been estimated to mediate >97% of GABAR-mediated inhibition of CGCs and thus play a major role in regulating information flow-through the cerebellar cortex (26). Here we have extended these previous studies on *stg* mice, utilizing a more appropriate background control mouse strain, to investigate what effects the stargazer mutation has on all cerebellar GABAR subtypes and subunits expressed and further to elucidate the cellular context of these abnormalities, *e.g.* are they restricted to CGCs? If so, are these abnormalities evident in all CGCs in each cerebella lobule? Finally, we aimed to establish at what subcellular level these abnormalities are translated and to address whether the effects we report were because of specific effects on expression of unique GABAR subtype(s)/subunit(s) or an overall consequence of aberrant CGC maturation.

Cerebellar GABARs can be broadly subclassified as being either γ2-containing or δ-containing. These mutually exclusive GABAR subtypes constitute 98% of the total number of GABARs expressed in the adult mouse cerebellum (34). Taking account of the quantitative data of Poltl *et al.* (34), it is evident that 57.3% of all GABARs in the cerebellum of mice contain α6 subunits. Approximately half of these (29.2% of total GABARs) contain γ2 and half (28.1% of total GABARs) δ subunits. Because 28.9% of all GABARs in the cerebellum contain δ subunits, nearly all of the δ subunit-containing GABARs must also contain α6 subunits. Based on our Western blotting data (Fig. 7) *stg* CGCs express only ~50% of the number of α6 receptors expressed by +/+, and this would theoretically equate to a reduction of 28.7% of total GABARs expressed by +/+ (34), which is completely compatible with the 30 ± 6% reduction in muscimol binding we report here (Fig. 1). Two pieces of evidence indicate that *stg* CGCs express only ~50% as many δ-containing GABARs as +/+. First, our Western blotting data showed that δ-immunoreactivity in *stg* cerebellum was only 51.6 ± 2.9% of +/+ (Fig. 7). Second, muscimol autoradiography which highlights $\alpha6\beta x\gamma2 + \alpha6\beta x\delta$ GABARs in the cerebellum (28, 40) identified that *stg* CGCs express 46 ± 6% fewer $\alpha6\beta x\gamma2 + \alpha6\beta x\delta$ GABARs compared with +/+. Allied to the fact that *stg* CGCs express 43 ± 8% fewer BZ-IS-binding sites (specifically $\alpha6\beta\gamma2$ receptors, Fig. 3), we can surmise that there are only ~50% of the $\alpha6\beta\gamma2$ and ~50% of the $\alpha6\beta\delta$ receptors expressed in *stg* CGCs compared with +/+. This fits with the 60% decrease in furosemide sensitivity in *stg* CGCs. Furthermore, we found that the relative proportion of α1, γ2, and δ subunits co-assembled with α6 isolated from +/+ and *stg* cerebella were identical (Table 2) indicating that although the number of α6-containing receptors expressed by *stg* CGCs is lower than in +/+ their subunit composition is identical. This is not the case however for the δ-containing receptors. The relative signal intensity of α6 subunits in δ-containing GABARs is similar in +/+ and *stg*, indicating that there is no significant change in the α6 subunit content of δ receptors. Control δ receptors comprise $\alpha6\beta\delta$, $\alpha1\alpha6\beta\delta$, and $\alpha1\beta\delta$ subtypes, which constitute 17.7, 10.4, and 0.8% of total GABAR numbers, respectively (34). Because we have established that the number of α6-containing receptors is lower by ~50% in *stg* but that the ratio of α6 subunit:δ subunit is unaltered indicates that the abundance of $\alpha6\beta\delta$ and $\alpha1\alpha6\beta\delta$ subtypes is ~50% of that found in +/+ (equivalent to $\alpha6\beta\delta$ and $\alpha1\alpha6\beta\delta$ subtypes comprising 8.9 and 5.2%, respectively, of total GABAR numbers expressed in +/+ cerebellum). However, the relative signal intensity of α1 subunits present in δ receptors is approximately double that found in *stg* (Table 2), indicating that the remaining δ receptors in *stg* contain twice as many α1 subunits. We can only assume that the abundance of $(\alpha1)_2\beta\delta$ GABARs is increased in *stg* CGCs. Because $\alpha1\beta\delta$ receptors contain two α1 subunits, $\alpha1\beta\delta$ receptors would need to constitute 3% of total GABARs expressed by +/+ CGCs to accommodate this observation, *i.e.* CGCs in *stg* would be expected to express ~4-fold as many $\alpha1\beta\delta$ receptors as +/+ CGCs.

We have found that the stargazer mutation selectively influences expression of the α6 subunit-containing subtypes. The abundance of the BZ-S subtype of GABARs is essentially unaffected. This subtype was found to have type I-like pharmacology based on zolpidem displacement of [^{3}H]Ro15-4513 binding to both +/+ and *stg* cerebellar membranes (Fig. 5), and thus is most likely representative of $\alpha1\beta x\gamma2$ GABARs in both *stg* and +/+ cerebella. This latter observation also implies that *stg* CGCs undergo a normal developmental program of GABAR maturation that is partially characterized by the transformation from type II BZ-S receptors (juvenile cerebellar GABARs, $\alpha2/\alpha3\beta\gamma2$ receptors) to type I BZ-S receptors (adult cerebellar GABARs). This argues against the notion that CGCs are restrained in an immature state in *stg* (17). Hence, our data suggest that the stargazer mutation selectively affects expression of the CGC-specific GABAR subtypes, $\alpha6\beta x\gamma2$, which has the potential to be targeted to and anchored at GABAergic synapses to respond in a neurosteroid-sensitive, zinc-insensitive manner to phasically released GABA (10, 18, 25, 26), and the extrasynaptically segregated $\alpha6\beta x\delta$ subtype that responds to tonic and synaptic over-spill

levels of GABA in a neurosteroid-insensitive, zinc-sensitive manner (10, 18, 25, 26). This was confirmed by *in situ* EM immunogold-labeling studies where CGC-specific $\alpha6$-containing GABARs ($\alpha6\beta x\delta + \alpha6\beta x\gamma2$) were found to be dramatically reduced at both extrasynaptic (largely $\alpha6\beta x\delta$) and synaptic ($\alpha6\beta x\gamma2$) loci (Fig. 8). The reduction in $\alpha6$ labeling of *stg* membranes by this route, however, was much more dramatic than expected from our other results and may be due to difficulties in extracting quantitative data from cell surface-clustered proteins whose accessibility, with relatively large reporter molecules such as gold particles, may be compromised if the fewer receptors expressed form smaller clusters or occupy more central aspects of the synapse. Clearly, the downstream consequences of the stargazer mutation modulate $\alpha6$-containing receptor expression, selectively. Finally, we propose that aberrant expression of the $\alpha6$ subunit is the primary cause of compromised GABAR expression in *stg*. Our rationale is based on the fact that ~50% fewer $\alpha6$ subunits are expressed by *stg* CGCs, which translates into ~50% fewer $\alpha6\beta\gamma2$ receptors and ~50% fewer $\alpha6\beta\delta$ receptors, *i.e.* both of these receptor types seem to be equally affected. If compromised expression of the δ subunit were the primary cause, we would anticipate that there would be no effect on the number of $\alpha6\beta\gamma2$ receptors. This posit is verified by our RT-PCR analysis that showed that the steady-state level of GABAR $\alpha6$ subunit mRNA was ~50% of that determined in +/+, whereas the steady-state level of GABAR δ subunit mRNA was not significantly different from +/+ (Fig. 7*B*). This suggests that the impaired expression of both synaptic and extrasynaptic $\alpha6$ subunit-containing GABARs is because of stargazer mutation-evoked reduction in the steady-state level expression of $\alpha6$ subunit mRNA.

Thus, we have shown that the inability to express functional AMPARs at the mossy fiber-CGC synapse of stargazer mice (7) has severe deleterious effects on the GABAR-inhibitory potential of these neurons *in vivo*. Heynen *et al.* (36) showed that selectively blocking $\alpha6$-containing GABARs with furosemide in rat cerebellar slices evoked a >2-fold increase in the gain of transmission of information from mossy fibers to granule cells. This would be perceived as a disadvantage because this would potentially increase the number of cerebellar granule cells that are simultaneously activated by specific mossy fiber afferent pathway inputs thus reducing the potential for motor program storage in the cerebellum. It would appear then that the GABAR-mediated inhibitory potential of CGCs is titrated according to the excitatory input these neurons experience, a phenomenon proposed by others in other neuronal networks (10, 12). We propose that expression and assembly of $\alpha6$-containing GABARs is regulated either directly by AMPAR-mediated excitability of CGCs, *e.g.* depolarization-mediated regulation of $\alpha6$ expression through a Ca^{2+}-mediated signal transduction pathway has already been proposed (45) and verified by us,[8] or indirectly as a downstream consequence of the loss of AMPAR activity, *e.g.* an inability to express BDNF (4, 5), and BDNF has been shown to regulate $\alpha6$ gene transcription (46). We have found that TARP$\gamma2$ and AMPAR subunits *e.g.* GluR2, are expressed in maturing CGCs *in vitro* from +/+ mice prior to expression of both $\alpha6$ and δ subunits and that expression of these subunits are regulated by AMPAR activity.[8] Furthermore, we have shown previously that GABAR profiles expressed by CGCs *in vitro* were dramatically modified by culturing under polarized (5 m$_M$ KCl) or depolarized, electrically silent conditions (25 m$_M$ KCl) (11); in the latter $\alpha6$ subunit mRNA steady-state level and protein expression were severely compromised implying that failure to express functional AMPARs and subsequent loss of electrical activity of CGCs in *stg* may play a part in the GABAR deficits observed in *stg* CGCs. Gault and Siegel (47, 48) identified that GABAR δ subunit mRNA was up-regulated in rat CGCs by a depolarization-dependent mechanism that involved Ca^{2+} influx through L-type voltage-gated calcium channels and/or NMDA receptors and subsequent calmodulin kinase activation. Down-regulation of GABAR δ subunit protein in the absence of AMPA receptor activity in *stg* CGCs, however, occurs in the absence of any change in its steady-state mRNA level. The GABAR $\alpha6$ knock-out mouse also fails to express δ subunit protein

in the cerebellum despite transcribing δ subunit mRNA to control level (28). This is thought to occur because the $\alpha6$ subunit is the preferred receptor assembly partner in CGCs, in the absence of $\alpha6$ subunit ($\alpha6$ subunit knock-out mouse), or when its expression is compromised (stargazer mouse) the amount of available receptor partner is reduced, and the δ protein that fails to assemble into a receptor is then rapidly turned over. The apparent up-regulation of $\alpha1\beta\delta$ receptors by *stg* CGCs appears to be insufficient to compensate for the loss of $\alpha6\beta\delta$ receptors because δ expression (Western blots, see Fig. 7) is reduced. Where $\alpha1\beta\delta$ receptors are trafficked/targeted and what role they play in inhibitory neurotransmission are currently unknown.

It is intriguing also to note that expression of $\alpha1$ and $\gamma2$ subunits and the BZ-S subtype of GABARs in CGCs is largely unaffected by the inability of *stg* CGCs to express functional AMPARs. What functional role these receptors play in the CGCs and how their expression is regulated remains to be resolved. We are currently investigating how AMPAR activity regulates expression, assembly, and trafficking of $\alpha6$-containing GABARs in CGCs.[8]

Acknowledgments

REFERENCES

1. Letts VA, Felix R, Biddlecome GH, Arikkath J, Mahaffey CL, Valenzuela A, Bartlett FS II, Mori Y, Campbell KP, Frankel WN. Nat. Genet. 1998; 19:340–347. [PubMed: 9697694]

2. Sharp AH, Black JL III, Dubel SJ, Sundarraj S, Shen J-P, Yunker AMR, Copeland TD, McEnery MW. Neuroscience. 2001; 105:599–617. [PubMed: 11516827]

3. Ives JH, Fung S, Tiwari P, Payne HL, Thompson CL. J. Biol. Chem. 2004; 279:31002–31009. [PubMed: 15136571]

4. Qiao X, Hefti F, Knusel B, Noebels JL. J. Neurosci. 1998; 16:640–648. [PubMed: 8551348]

5. Qiao X, Chen L, Gao H, Bao S, Hefti F, Thompson RF, Knussel B. J. Neurosci. 1998; 18:6990–6999. [PubMed: 9712667]

6. Di Pasquale E, Keegan KD, Noebels JL. J. Neurophysiol. 1997; 77:621–631. [PubMed: 9065835]

7. Chen L, Chetkovich DM, Petralia RS, Sweeney NT, Kawasaki Y, Wenthold RJ, Bredt DS, Nicoll RA. Nature. 2000; 408:936–943. [PubMed: 11140673]

8. Rouach N, Byrd K, Petralia RS, Elias GM, Adesnik H, Tomita S, Karimzadegan S, Kealey C, Bredt DS, Nicoll RA. Nat. Neurosci. 2005; 8:1525–1533. [PubMed: 16222232]

9. Tomita S, Chen L, Kawasaki Y, Petralia RS, Wenthold RJ, Nicoll RA, Bredt DS. J. Cell Biol. 2003; 161:805–816. [PubMed: 12771129]

10. Nusser Z, Sieghart W, Somogyi P. J. Neurosci. 1998; 18:1693–1703. [PubMed: 9464994]

11. Ives JH, Drewery DL, Thompson CL. Neuropharmacol. 2002; 43:715–725.

12. Leroy C, Poisbeau P, Keller AF, Nehlig A. J. Physiol. (Lond.). 2004; 557:473–487. [PubMed: 15034126]

13. Peng Z, Huang CS, Stell BM, Mody I, Houser CR. J. Neurosci. 2004; 24:8629–8639. [PubMed: 15456836]

14. Yamada MK, Nakanishi K, Ohba S, Nakamura T, Ikegaya Y, Nishiyama N, Matsuki N. J. Neurosci. 2002; 22:7580–7585. [PubMed: 12196581]

15. Jovanovic JN, Thomas P, Kittler JT, Smart TG, Moss SJ. J. Neurosci. 2004; 24:522–530. [PubMed: 14724252]

16. Elmariah SB, Crumling MA, Parsons TD, Balice-Gordon RJ. J. Neurosci. 2004; 24:2380–2393. [PubMed: 15014113]

17. Chen L, Bao S, Qiao X, Thompson RF. Proc. Natl. Acad. Sci. U. S. A. 1999; 96:12132–12137. [PubMed: 10518588]

18. Tia S, Wang JF, Kotchabhakdi N, Vicini S. J. Neurosci. 1996; 16:3630–3640. [PubMed: 8642407]

19. Korpi ER, Uusi-Oukari M, Kaivola J. Neuroscience. 1993; 53:483–488. [PubMed: 8388087]

20. Zheng T, Santi M-R, Bovolin P, Marlier LN, Grayson DR. Dev. Brain Res. 1993; 75:91–103. [PubMed: 8222213]

21. Thompson CL, Stephenson FA. J. Neurochem. 1994; 62:2037–2044. [PubMed: 8158152]

22. Thompson CL, Pollard S, Stephenson FA. Neuropharmacol. 1996; 35:1337–1346.

23. Thompson CL, Jalilian Tehrani M, Barnes EM Jr. Stephenson FA. Mol. Brain Res. 1998; 60:282–290. [PubMed: 9757064]

24. Brickley SG, Cull-Candy SG, Farrant M. J. Physiol. (Lond.). 1996; 497:753–759. [PubMed: 9003560]

25. Brickley SG, Cull-Candy SG, Farrant M. J. Neurosci. 1999; 19:2960–2973. [PubMed: 10191314]

26. Hamann M, Rossi DJ, Attwell D. Neuron. 2002; 33:625–633. [PubMed: 11856535]

27. Hashimoto K, Fukaya M, Qiao X, Sakimura K, Watanabe M, Kano M. J. Neurosci. 1999; 19:6027–6036. [PubMed: 10407040]

28. Jones A, Korpi ER, McKernan RM, Pelz R, Nusser Z, Makela R, Mellor JR, Pollard S, Bahn S, Stephenson FA, Randall AD, Sieghart W, Somogyi P, Smith AJH, Wisden W. J. Neurosci. 1997; 17:1350–1362. [PubMed: 9006978]

29. Drescher DG, Green GE, Khan KM, Hajela K, Beisel KW, Morley BJ, Gupta AK. J. Neurochem. 1993; 61:1167–1170. [PubMed: 8395561]

30. Jechlinger M, Pelz R, Tretter V, Klausberger T, Sieghart W. J. Neurosci. 1998; 18:2449–2457. [PubMed: 9502805]

31. Slany A, Zezula J, Tretter V, Sieghart W. Mol. Pharmacol. 1995; 48:385–391. [PubMed: 7565617]

32. Tretter V, Ehya N, Fuchs K, Sieghart W. J. Neurosci. 1997; 17:2728–2737. [PubMed: 9092594]

33. Thompson CL, Drewery DL, Atkins HD, Stephenson FA, Chazot PL. Neurosci. Lett. 2000; 283:85–88. [PubMed: 10739881]

34. Poltl A, Hauer B, Fuchs K, Tretter V, Sieghart W. J. Neurochem. 2003; 87:1444–1455. [PubMed: 14713300]

35. Pollenz RS. ECL Highlights. 1996; 9:2–3.

36. Heynen AJ, Quinlan EM, Bae DC, Bear MF. Neuron. 2000; 28:527–536. [PubMed: 11144361]

37. Lucocq, JM. Fine Structure Immunocytochemistry. Springer-Verlag; Berlin: 1993. p. 279-302.

38. Lucocq JM. J. Anat. 1994; 184:1–13. [PubMed: 8157482]

39. Lowry OH, Rosebrough NJ, Farr AL, Randall RJ. J. Biol. Chem. 1951; 193:265–275. [PubMed: 14907713]

40. Mihalek RM, Banerjee PK, Korpi ER, Quinlan JJ, Firestone LL, Mi Z-P, Lagenauer C, Tretter V, Sieghart W, Anagnostaras SG, Sage JR, Fanselow MS, Guidotti A, Spigelman I, Li Z, DeLorey TM, Olsen RW, Homanics GE. Proc. Natl. Acad. Sci. U. S. A. 1999; 96:12905–12910. [PubMed: 10536021]

41. Laurie DJ, Wisden W, Seeburg PH. J. Neurosci. 1992; 12:4151–4172. [PubMed: 1331359]

42. Korpi ER, Kuner T, Seeburg PH, Luddens H. Mol. Pharmacol. 1995; 47:283–289. [PubMed: 7870036]

43. Wafford KA, Thompson SA, Thomas D, Sikela J, Wilcox AS, Whiting PJ. Mol. Pharmacol. 1996; 50:670–678. [PubMed: 8794909]

44. Brickley SG, Revilla V, Cull-Candy SG, Wisden W, Farrant M. Nature. 2001; 409:88–92. [PubMed: 11343119]

45. Suzuki K, Sato M, Morishima Y, Nakanishi S. J. Neurosci. 2005; 25:9535–9543. [PubMed: 16221864]

46. Bulleit RF, Hsieh T. Dev. Brain Res. 2000; 119:1–10. [PubMed: 10648867]

47. Gault LM, Siegel RE. J. Neurosci. 1997; 17:2391–2399. [PubMed: 9065500]

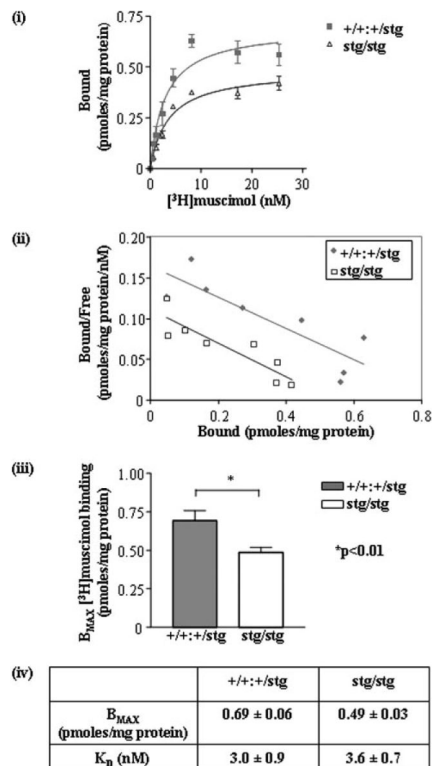48. Gault LM, Siegel RE. J. Neurochem. 1998; 70:1907–1915. [PubMed: 9572274]

FIGURE 1. [^{3}H]Muscimol binding to control (+/+) and stargazer (*stg*) cerebellar membrane homogenates

i, plot of [^{3}H]muscimol (0.540 n$_M$) saturation binding data to +/+ and *stg* cerebellar membranes ($\gamma 2 + \delta$-containing GABARs) from one of two assays conducted. *ii*, Rosenthal transformation of specific [^{3}H]muscimol binding data to +/+ and *stg* cerebellar membrane homogenates shown in *i*. *iii*, bar graph demonstrates the difference in B_{max} values calculated for [^{3}H]muscimol binding to +/+ and *stg* cerebellar membranes. Results show a reduction to $70 \pm 6\%$ of +/+ levels in B_{max}, *i.e.* total binding sites in *stg* cerebellar membranes. *iv, table* summarizing calculated and K_D values for [^{3}H]muscimol binding to +/+ and *stg* cerebellar membranes from two separate assays. Data are means $\pm$ S.E. for assays performed in triplicate for two separate preparations ($n = 6$). Membrane homogenates were prepared from $n = 10$ cerebella per mouse strain in each assay.
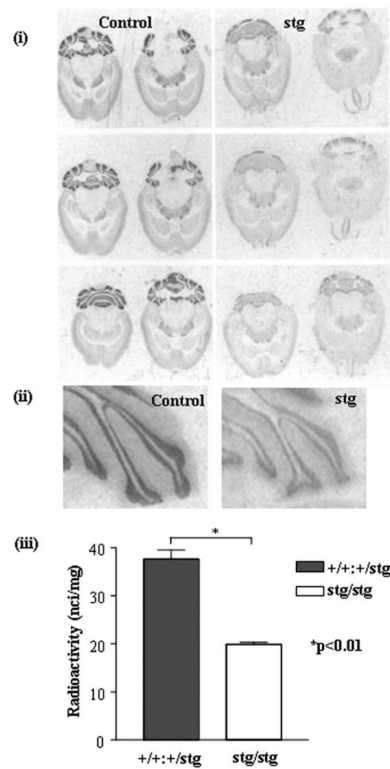
FIGURE 2. [³H]Muscimol binding to control (+/+) and stargazer (*stg*) adult mouse brain, *in situ* autoradiography

i, in situ autoradiography of [³H]muscimol ($\alpha6\beta\gamma2$, $\alpha1\alpha6\beta\gamma2$, $\alpha6\beta\delta$, and $\alpha1\alpha6\beta\delta$ GABARs) binding in +/+ and *stg* cerebella using a saturating concentration of [³H]muscimol (20 n$_M$). Nonspecific binding was determined by competitive displacement of muscimol with GABA (100 μ_M). The signal obtained under these latter conditions was at the level of film background. Six sections from different horizontal planes are shown to demonstrate that the loss of receptor expression was consistent throughout the cerebellum. *ii*, magnified image of cerebellar lobules labeled with [³H]muscimol. *iii, histogram* illustrating the results of quantitative image analysis of grayscale intensities using image J software to determine the relative amounts of ligand bound in the cerebellar granule cell layers. A dramatic, significant reduction (by $46 \pm 3\%$, $p < 0.01$) in [³H]muscimol binding in the cerebellar granule cell layer of *stg* was determined. Data shown are representative of at least three +/+ and three *stg* brains and a minimum of 10 sections per brain.
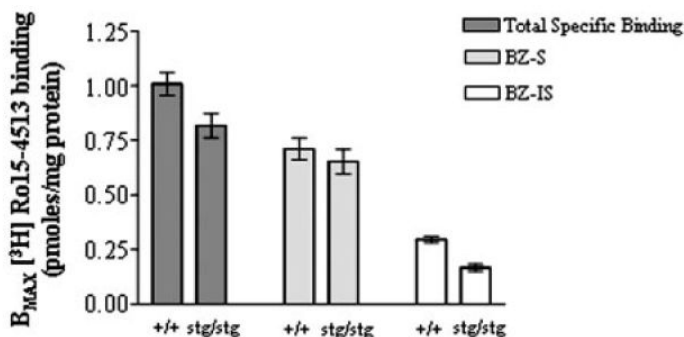
	+/+:+/stg	stg/stg
Total Binding B_{MAX}(pmoles/mg protein)	1.01 ± 0.05	0.82 ± 0.06 ($-19 \pm 8\%$)
K_D(nM)	3.8 ± 0.7	4.2 ± 1.0
BZ-S B_{MAX}(pmoles/mg protein)	0.71 ± 0.08	0.65 ± 0.06 ($-9 \pm 14\%$)
K_D(nM)	3.3 ± 0.8	4.1 ± 1.2
BZ-IS B_{MAX}(pmoles/mg protein)	0.30 ± 0.01	0.17 ± 0.02 ($-43 \pm 8\%$)
K_D(nM)	5.0 ± 0.8	5.1 ± 1.6

FIGURE 3. [³H]Ro15-4513 binding to control (+/+) and stargazer (*stg*) cerebellar membrane homogenates

Full saturation [³H]Ro15-4513 binding curves were generated using +/+ and *stg* cerebellar membranes and a concentration range of 0.3–40 n$_M$ [³H]Ro15-4513. Nonspecific binding was determined in the presence of Ro15-1788 (10 μ_M). [³H]Ro15-4513 binding in the presence of flunitrazepam (10 μ_M), defined BZ-IS-binding sites, and hence benzodiazepine-sensitive (BZ-S) sites could be determined by subtraction of the BZ-IS-binding sites from total [³H]Ro15-4513 specific binding sites. The *bar graph* illustrates the difference in B_{max} values calculated for [³H]Ro15-4513 binding to +/+ and *stg* membranes. Results show differences in B_{max} for total specific binding ($100 \pm 5\%$ and $81 \pm 7\%$), BZ-S binding ($100 \pm 11\%$ and $92 \pm 9\%$), and BZ-IS binding ($100 \pm 3\%$ and $57 \pm 12\%$) in +/+ and *stg* membranes, respectively. The *table* summarizes the estimated B_{max} and K_D values for [³H]Ro15-4513 binding to +/+ and *stg* cerebellar membranes. Data are representative of the mean ± S.E. for assays conducted in triplicate on two separate membrane preparations per mouse strain ($n = 6$). Ten cerebella were used for each preparation per mouse strain.
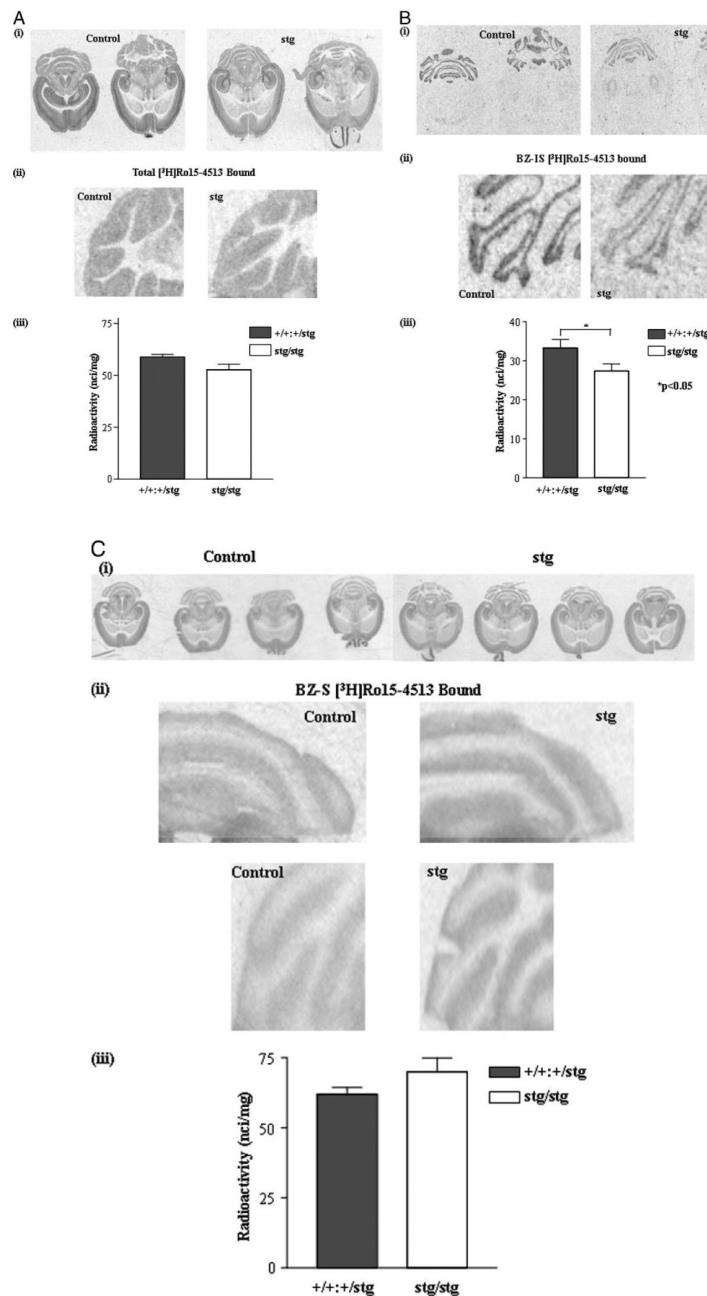
FIGURE 4. [³H] Ro15-4513 binding to control (+/+) and stargazer (*stg*) adult mouse brain; *in situ* autoradiography

A, total [³H]Ro15-4513 binding. *Panel i, in situ* autoradiography of total [³H]Ro15-4513 binding (γ2-containing GABARs) to +/+ and *stg* cerebella using a near-saturating concentration of [³H]Ro15-4513 (20 nM). Nonspecific binding was determined by competitive displacement of Ro15-4513 with the benzodiazepine receptor antagonist, Ro15-1788 (10 μM). The signal obtained under these latter conditions was at the level of film background. Two representative comparable sections per mouse strain are shown. *Panel ii*, magnified image of cerebellar lobules labeled with [³H]Ro15-4513. *Panel iii, histogram* illustrating the results of quantitative image analysis of grayscale intensities using image J software to determine the relative amounts of ligand bound in the cerebellar granule cell

layers. A small ($10 \pm 4\%$) but insignificant ($p > 0.05$) reduction in total [^{3}H]Ro15-4513 binding in the cerebellar granule cell layer of *stg* was determined. Data shown are representative of at least three +/+ and three *stg* brains and a minimum of 10 sections per brain. *B*, BZ-IS [^{3}H]Ro15-4513 binding. *Panel i, in situ* autoradiography of flunitrazepam (10 μM)-insensitive [^{3}H]Ro15-4513 (BZ-ISR) binding ($\alpha6\beta\gamma2$, $\alpha1\alpha6\beta\gamma2$ GABARs) in +/+ and *stg* cerebella using a saturating concentration of [^{3}H]Ro15-4513 (20 nM). Nonspecific binding was determined by competitive displacement of Ro15-4513 with benzodiazepine receptor antagonist, Ro15-1788 (10 μM). The signal obtained under these conditions was at the level of film background. *Panel ii*, magnified image of cerebellar lobules following autoradiography to identify BZ-ISRs. *Panel iii, histogram* illustrating the results of quantitative image analysis of grayscale intensities using image J software to determine the relative amounts of radioligand bound in the cerebellar granule cell layer. A small but significant reduction (by $21 \pm 7\%$; $p < 0.05$) in flunitrazepam-insensitive [^{3}H]Ro15-4513 binding in the cerebellar granule cell layer of *stg* was determined. Data shown are representative of at least three +/+ and three *stg* brains and a minimum of 10 sections per brain. *C*, BZ-S [^{3}H]flunitrazepam binding. *Panel i, in situ* autoradiography of [^{3}H]flunitrazepam (BZ-SR) binding (*e.g.* $\alpha1\beta\gamma2$ GABARs) in +/+ and *stg* cerebella using [^{3}H]flunitrazepam (5 nM). Nonspecific binding was determined by competitive displacement of flunitrazepam with benzodiazepine receptor antagonist, Ro15-1788 (10 μM). The signal obtained under these conditions was at the level of film background. *Panel ii*, magnified image of cerebellar lobules following autoradiography to identify BZ-SRs. *Panel iii, histogram* illustrating the results of quantitative image analysis of grayscale intensities using image J software to determine the relative amounts of radioligand bound in the cerebellar granule cell layer. A small, nonsignificant increase (by $13 \pm 6\%$; $p > 0.05$) in [^{3}H]flunitrazepam binding in the cerebellum of *stg* was determined.
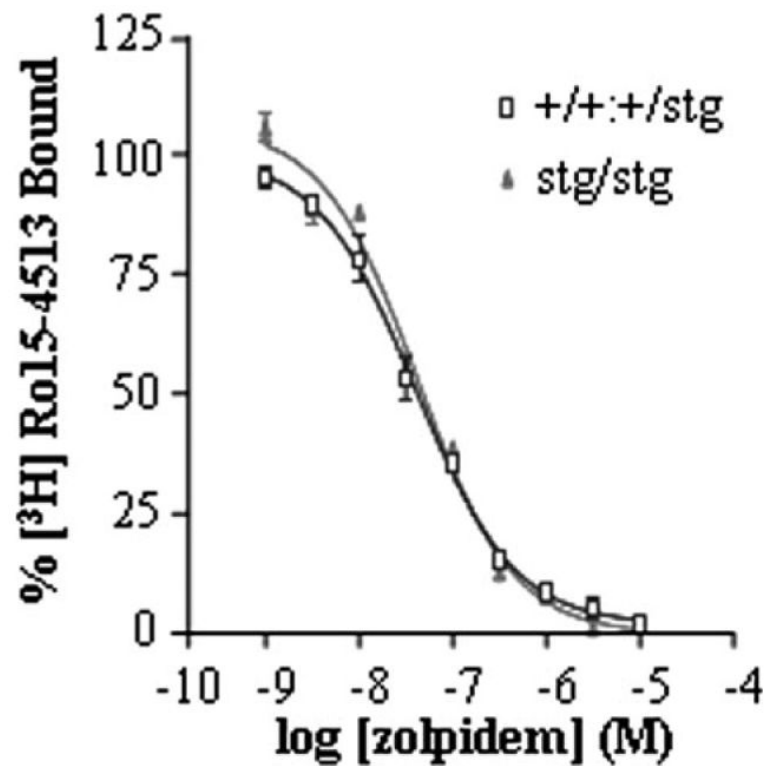
FIGURE 5. Zolpidem displacement of [^{3}H]Ro15-4513 binding to adult control (+/+) and stargazer (*stg*) cerebellar membrane homogenates
Zolpidem (1 nM to 10 μM) was used to competitively displace BZ-S [^{3}H]Ro15-4513 (5 nM) equilibrium binding from cerebellar membrane homogenates derived from adult +/+ and *stg* mice. [^{3}H]Ro15-4513 binding displaced by flunitrazepam (10 μM) defined benzodiazepine-sensitive (*BZ-S*) sites. 100% binding was that obtained in the absence of competitive ligand.

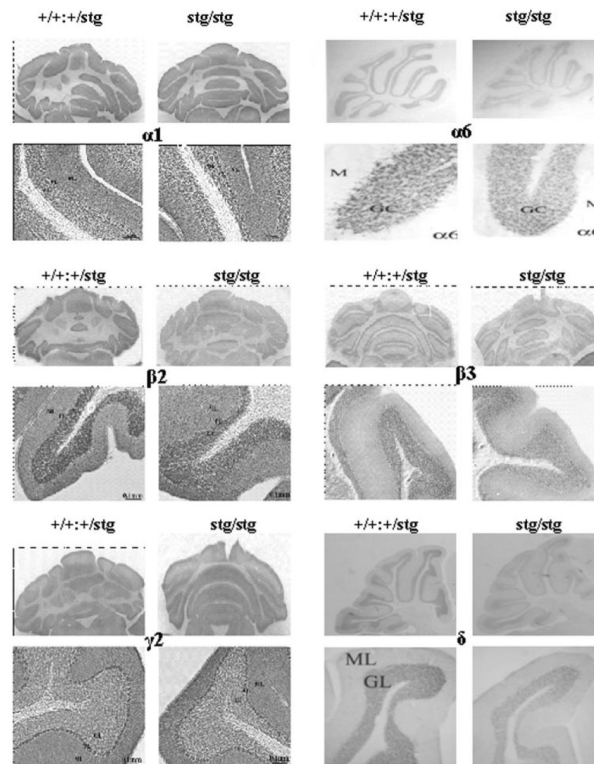**FIGURE 6. Immunohistochemical mapping of GABAR α1, α6, β2, β3, γ2, and δ subunits in the cerebellum of control (+/+) and stargazer (*stg*) mice**
Adult +/+ and *stg* mice were perfusion-fixed with paraformaldehyde, cryostat-sectioned, and immunostained as described under "Experimental Procedures." Anti-GABAR subunit-specific antibodies were optimized for signal:noise ratio. Final concentrations used were α1 (0.5 μg/ml), α6 (0.06 μg/ml), β2 (0.5 μg/ml), β3 (0.5 μg/ml), γ2 (0.5 μg/ml), and δ (0.25 μg/ml). Each panel shows a low power image of an immunostained whole cerebellar section and a high power image cross-section of a typical cerebellar lobule from each mouse strain. These are representative results derived from a minimum of three +/+ and three *stg* brains. *ML*, molecular layer; *GL*, granular layer.
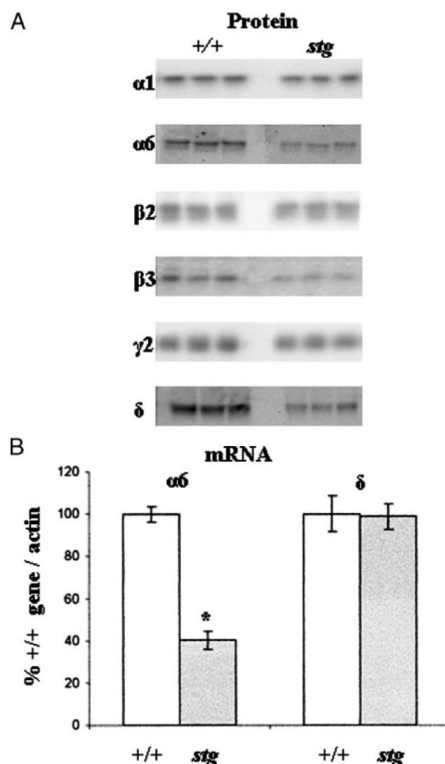
FIGURE 7.

A, Western blot analysis indicating changes in the abundance of GABAR subunits expressed in control (+/+) and stargazer (*stg*) cerebella. Immunoblots show the analysis of the six predominant GABAR subunits known to be present in cerebellar membranes of three +/+ and three *stg* mice. There was a large decrease in the intensity of the immunoreactive bands for the α6 (49 ± 2%) and δ (52 ± 3%) subunits and a weaker decrease in α1 (85 ± 1%), β2 (85 ± 2%), and β3 (64 ± 5%) subunits in *stg* cerebella $p < 0.01$. No significant changes in the intensity of the bands for γ2 (95 ± 4%) subunit were observed in *stg* cerebella $p > 0.05$. *B*, semi-quantitative RT-PCR amplification of cerebellar α6 and δ GABAR subunits mRNAs transcribed by control (+/+) and stargazer (*stg*) mice. Primer pairs specific for GABAR subunits α6 and δ cDNAs were designed as described previously (11, 29). In each case 1.0, 0.6, 0.4, 0.2, 0.1, and 0.05 μg of total RNA isolated from +/+ and *stg* cerebellum was reverse transcribed (*RT*) in a total volume of 35 μl of RT mix. 2 μl of each cDNA sample was removed for PCR amplification. Optimized amplification strategies were designed for each subunit cDNA. Following separation on a 1.2% (w/v) agarose gel and ethidium bromide staining, PCR products were visualized under UV light, and band image intensity was measured. The levels of the GABAR subunit mRNAs transcribed were normalized for β-actin mRNA transcription. Relative GABAR subunit mRNA levels found in +/+ and *stg* cerebellum are shown. Messenger RNA was isolated from a minimum of two +/+ and two *stg* mice. RT-PCR experiments were performed a minimum of three times each. *Asterisk* indicates significant difference ($p < 0.05$).
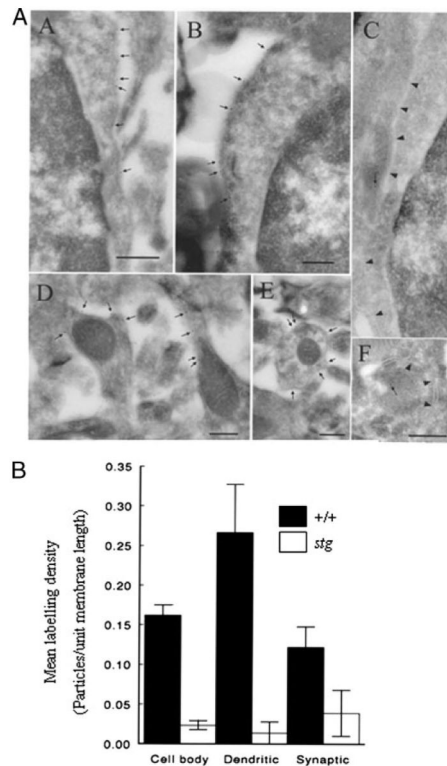
FIGURE 8. Postembedding immunocytochemistry on electron microscopic sections
A, immunolabeling of GABAR a6 subunit in the cerebellar granule cell layer of +/+ (*panels A, B, D*, and *E*) or *stg* (*panels C* and *F*) mouse cerebellum. The plasma membrane of granule cell bodies from +/+ mice (*panels A* and *B*) are labeled by gold particles (*arrows*), but the plasma membrane of *stg* mice (*panel C*; *arrowheads*) are not labeled, and the *arrow* in *panel C* marks a gold particle representing nonspecific-labeling of a mitochondrial profile. Plasma membrane of a dendrite (containing mitochondrial profiles) from +/+ mice is strongly labeled but those from *stg* mice are not labeled (*arrow* in *panel F* represents background labeling over a mitochondrial profile). *Bars* represent 500 nm in *A* and 250 nm in *panels B–F*. Two +/+ and two *stg* brains were fixed by each perfusion method. *B*, quantitative analysis of mean labeling density (number of gold particles/unit membrane length) of GABAR a6 immunoreactivity in various extrasynaptic (soma and dendrites) and synaptic subdomains of cerebellar granule cells from +/+ (*closed boxes*) and *stg* mice (*open boxes*) *in situ*. Data are representative of the mean ± S.E.
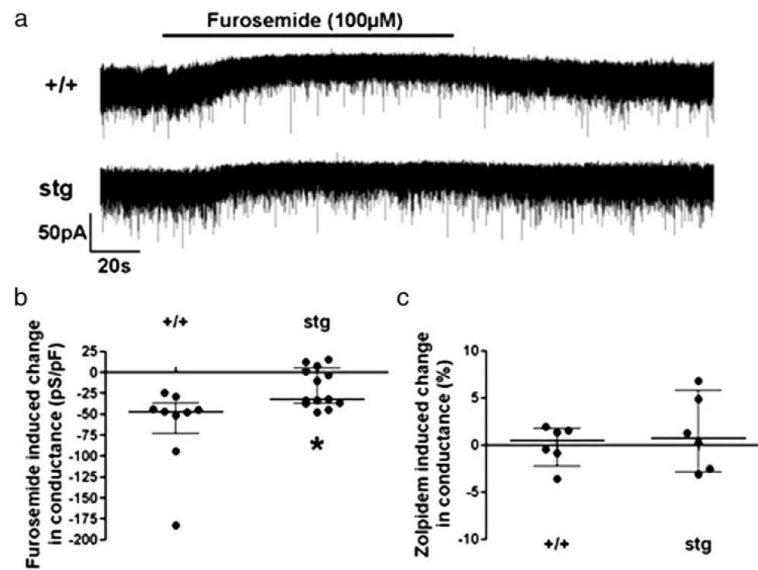
FIGURE 9. The tonic GABA$_A$ receptor-mediated current in epileptic stargazer (*stg*) CGC is mediated by a smaller percentage of α6-containing GABARs
a, representative traces showing the reduction in holding current induced by the application of the α6/α4 antagonist furosemide, and the different sensitivity in +/+ and *stg* mice. *b*, scatter plot showing that furosemide reduces whole-cell conductance significantly more in +/+ mice than *stg* mice (+/+, −47 (interquartile range, −73, −36) pS/pF; *stg*, −19 (−37, 4) pS/pF; n = 9–13, p = 0.011, Mann Whitney test). *c*, zolpidem produces no significant change in whole-cell conductance in either *stg* or +/+ mice (+/+, 0.4 (−2, 2) %, n = 6, p = 0.8; *stg*, 0.7, (−3, 6) %, n = 6, p = 0.6, Wilcoxon matched pairs test).

TABLE 1

Quantification of GABAR subunit proteins by Western blot analysis of cerebellar membranes derived from adult stargazer (*stg*) mouse cerebella relative to age-matched controls (+/+)

Equal amounts of cerebellar membrane protein from age-matched adult +/+ and *stg* mice were separated by SDS-PAGE and subjected to Western blot analysis, and immunoreactive band intensities were determined by ImageJ analysis as described under "Experimental Procedures." Results were obtained from three to six +/+ and three to six *stg* mice that were investigated a total of three to five times and are expressed as percentages of the weighted average subunit level found in +/+ mice ± S.E. For statistical comparison unpaired Student's *t* test was used. *n* indicates number of individual animals tested; NS indicates not significant.

Protein	+/+ = 100% (mean ± S.E.)	n	*stg* % of +/+ (mean ± S.E.)	n	Significance (*p* value)
α1	100 ± 2	3	85 ± 1	3	<0.001
α6	100 ± 3	6	49 ± 2	6	<0.0001
β2	100 ± 3	3	85 ± 2	3	<0.01
β3	100 ± 3	3	64 ± 5	3	<0.001
γ2	100 ± 2	3	95 ± 4	3	NS
δ	100 ± 2	6	52 ± 3	6	<0.0001

TABLE 2

Estimation of the relative α1, α6, γ2, and δ subunit composition of α6- and δ-containing GABARs in control (+/+) and stargazer (*stg*) cerebellum

Cerebella from adult control (+/+) and *stg* mice were extracted with deoxycholate buffer. Equivalent amounts of extracted protein from each mouse were either incubated with δ or α6 antibodies, and the precipitated proteins were subjected to immunoblotting using digoxigenized α1, α6, γ2, or δ antibodies as probes. Immunoreactive proteins were identified by chemiluminescence, and intensity of protein staining was quantified using Fluor-S multi-imager (Bio-Rad). Since staining efficiency of individual subunit depends on the number of epitopes recognized by the antibodies as well as their avidity, intensity of protein staining cannot be used for direct quantification of subunits. A possible change in the subunit composition of the precipitated receptors can, however, be determined when the signal intensity of the co-precipitated subunit is referred to that of the precipitated subunit in +/+ and stargazer cerebellum. Data are from two experiments performed with two +/+ and two *stg* mice in duplicate. For statistical comparison unpaired Student's *t* test was used (NS indicates not significant, not detected).

δ IP	+/+, % of δ	*stg*, % of δ	Significance (*p* value)
δ	100 ± 4	100 ± 2	
α6	45 ± 16	40 ± 13	NS
α1	43 ± 8	117 ± 11	<0.05
γ2			NS

α6 IP	% of α6	% of α6	
α6	100 ± 3	100 ± 8	
α1	151 ± 19	175 ± 12	NS
γ2	114 ± 11	138 ± 16	NS
δ	141 ± 14	133 ± 13	NS